Attitude Stabilization for Lunar and Planetary Lander with Variable Damper

Takao Maeda[a]

Nagoya University, Nagoya, 464-8603, Japan

Masatsugu Otsuki[b] and Tatsuaki Hashimoto[c]

Japan Aerospace Exploration Agency, Sagamihara, 252-5210, Japan

Susumu Hara[d]

Nagoya University, Nagoya, 464-8603, Japan

This paper describes an attitude control method that has been designed to prevent the overturning of lunar and planetary landers, based on a variable-damping shock absorber for the landing gear. Conventionally, the landing gear of lunar and planetary landers has a fixed shock attenuation parameter that is not used proactively for attitude control of the lander during the touchdown sequence. The new method enables the suppression of any disturbance to the attitude of the lander by adjusting the damping coefficient of each landing leg independently, based on the angular velocity vector and displacement velocity of each leg of the lander. The results of a numerical simulation indicate that the control rule for a three-dimensional system is effective for preventing the overturning of the lander on inclined terrain. The results of the simulation and experiments show that the landing gear with the actively variable damping and the control rule play a major role in preventing the overturning of a lunar or planetary lander.

[a] Postdoctoral Researcher, Graduate School of Engineering, Furo-cho, Chikusa-ku, Nagoya.

[b] Assistant Professor, Institute of Space and Astronautical Science, 3-1-1 Yoshinodai, Chuo-ku, Kanagawa

[c] Professor, Institute of Space and Astronautical Science, 3-1-1 Yoshinodai, Chuo-ku, Kanagawa

[d] Professor, Graduate School of Engineering, Furo-cho, Chikusa-ku, Nagoya.

Nomenclature

c_i = damping coefficient of right and left damper Ns/m

c_{nom} = nominal damping coefficient of damper Ns/m

c_T = damping coefficient of terrain surface, Ns/m

d_i = displacement length of right and left of damper, m

$\boldsymbol{f}$ = total force, N

$\boldsymbol{f}_i$ = force acting on no.i leg, N

$\boldsymbol{f}_{Ri}$ = restricting force limiting the landing gear linear motion, N

$\boldsymbol{f}_{Si}$ = force from spring and damper of landing gear, N

g = gravitational acceleration of the Moon, m/s^2

H = Initial position height of center of mass of lander body, m

h = height of the center of mass of the lander body, m

i = index refers to each landing gear

$\boldsymbol{J}_i$ = moment of inertia matrix of lander body, kgm^2

k = spring constant of shock absorber, N/m

k_T = spring constant of terrain surface, N/m

$\boldsymbol{M}$ = matrix of mass, kg

m = mass of lander main body, kg

m_f = mass of landing leg and footpad, kg

N = number of landing legs

$\boldsymbol{R}_{\mathrm{body}}$ = position vector of center of the lander body, m

$\boldsymbol{R}_{Fi}$ = position vector of footpad, m

$\boldsymbol{R}_{Pi}$ = position vector of mounting position of the landing gear, m

$\boldsymbol{r}_i$ = point of application of the force from leg, m

$\boldsymbol{r}_{Si}$ = direction vector of the liner motion of landing leg

$\boldsymbol{s}_i$ = vector from footpad to the mounting position of the body, m

t = time step, s

V = Lyapunov function

w = circumscribed circle diameter of footpads, m

$\boldsymbol{\tau}$ = total torque, Nm

$\boldsymbol{\tau}_i$ = torque acting on lander body from no.i leg, Nm

λ = Lagrange multiplier

θ = tilt angle of lander main body, rad

μ' = dynamic frictional coefficient of soil

$\boldsymbol{\Phi}$ = equation of constraint condition

ϕ = terrain inclination angle, degree

ψ = twist angle between x axis of the lander and the direction of slope

or direction of the lander horizontal velocity, degree

$\boldsymbol{\omega}$ = angular velocity vector of lander body, rad/s

I. Introduction

To successfully touch down on the rough but interesting regions of Moon, Mars, other planets, their satellites, and also asteroids, there is a need for a robust landing gear system that could be adopted for future exploratory missions that involve landing on such a body. For example, as shown in Figure 1, the exploration of crater central hills, lunar lava tubes, highlands, or canyons will be necessary to obtain data that will be pivotal to determining the origins of the Earth and the Solar System [1–3]. These areas, however, feature a rough terrain with many slopes. To achieve a successful touchdown on such a rough terrain, there is a need for a landing system that can adapt to different kinds of slopes, steps, and obstacles. However, it is difficult to design a landing system that could be applied to a wide variety of terrains. Conventional landing gear systems that have been adopted by previous Moon or Mars missions relied on plastic-deformation shock absorbers. The role of this landing gear was to attenuate the impact experienced at the end of the touchdown sequence. Therefore, materials capable of absorbing large amounts energy, such as aluminum honeycomb crush cores, have commonly been used. However, the features of these shock attenuation mechanisms were fixed according to their design values, and the parameters did not vary adaptively; this prevented their application to different types of terrain.

In practice, there are active, semi-active, and structurally engineered types of passive landing gear. Typical examples of such landing gear include the following: (1) Gear whereby the damper coefficient is controlled by the acceleration [4]; (2) Gear based on a servo-motor and the compliance of a control leg [5]; (3) Gear with a ball screw and predictive control[6]; (4) Momentum-exchange impact dampers [7, 8]; (5) Gear with a base-extension separation mechanism [9]; (6) Articulated landing gear for rotor craft that use robotic legs [10, 11]; (7) Self-leveling landing gear with a link and spring [12]. The aim of (1), (2), (4), and (5) is to reduce rebound. The systems of (1) and (2) reduce rebound by adjusting the landing gear compliance, while that of (3) uses a ball-screw driven landing gear to reduce the shock of landing. The systems of (4) and (5) rely on the principle of a mass damper to suppress rebound. The lander in (6) adjusts its attitude by articulating robotic landing legs. It aims to mitigate the peak acceleration experienced during landing by adopting jointed articulated-type landing legs, the stiffnesses of which are controlled based on the determination of
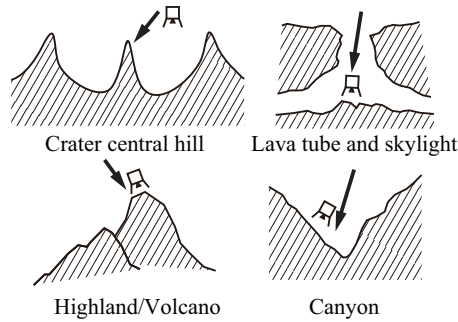
Fig. 1 Challenging landing locations for next generation of landing missions

contact between the legs and the ground, so as to enable the full utilization of the large load capacity of the rotor craft. The landing gear in (7) achieves self-leveling of the lander after touchdown by using passive tuned landing leg. Although these landing-gear systems suppress lander rebound or enable self-leveling after landing, they have not been applied to active control for preventing overturning utilizing information on the angular velocity of the lander.

In this study, we set out to devise a means of preventing a lander from overturning through the use of a variable damper as the shock absorber for the landing gear. In our proposal, we control only the damping coefficient of the landing leg. Each variable damper is controlled independently based on the lander state to prevent it from overturning. We verified the advantages of using a variable damper as the landing gear shock absorber [13]. However, that study was limited to two-dimensional plane motion. For this study, therefore, we set out to address the three-dimensional model to verify the validity of the variable damper and its control method. We evaluated three types of landing models through the application of numerical simulations: a conventional honeycomb crush core, a fixed damper, and a variable damper. In particular, the ability to successfully touch down on inclined terrain with the four-legged lander is discussed. Furthermore, the relationship between the stability of the lander on a slope and the number of landing legs is evaluated. Finally, the efficacy of the method proposed for controlling the variable shock attenuation mechanism for the landing gear is discussed.
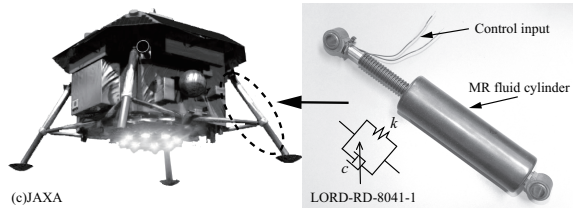
Fig. 2 Concept of landing gear with variable damper

II. Variable-damping landing gear

In this section, we describe the essential concept of variable-damping landing gear. To suppress the shock of landing, some type of shock-attenuation mechanism is required. For a touch-down on a completely horizontal flat surface, a soft landing leg, that is a landing leg with low damping coefficient, is suitable. However, for any touchdown on an incline, step, rocks, or other rough terrain, the landing gear should also be able to support the lander attitude. The landing leg must not be too soft as this would reduce the stability margin of the lander's attitude.

A passive landing gear, such as those based on a honeycomb crush core, spring-and-damper, or air-bag, should be designed to satisfy the shock attenuation and attitude stabilization requirements. However, it is not possible to optimize all of the performance parameters simultaneously. If the features of a shock attenuation mechanism could be controlled, however, these conflicting aims could be achieved. The variable damper constitutes one possible solution to this problem. A large damping coefficient can prevent the acceleration of the angular velocity of the lander on an inclined surface, while a small damping coefficient can reduce the shock acting on the leg that touches the surface first. Those are the essentials of overturning prevention control for landing gear with a variable damper. Details of the control method will be explained in the next section.

III. Control rule

Here, we discuss the control rule governing the lander attitude shown in Figure 3. Figure 4 shows the force that acts on landing gear i. In these figures, $\boldsymbol{f}_i$ is the total force acting on the landing gear, $\boldsymbol{f}_{Si}$ is the force from the spring and damper of the landing gear and $\boldsymbol{f}_{Ri}$ is the restricting force limiting the landing gear linear motion. Here, i is the index that refers to each landing gear.

6

The three-dimensional equation of motion for the lander main body is as follows:

$$\boldsymbol{J'\dot{\omega}'} = \boldsymbol{\tau}_i - \boldsymbol{\tilde{\omega}'J'\omega'}. \tag{1}$$

Here, the torque $\boldsymbol{\tau}_i$ is,

$$\boldsymbol{\tau}_i = \boldsymbol{\tilde{r}'f'}_i, \tag{2}$$

where $\boldsymbol{r}_i$ is the point of application of the force, $\boldsymbol{f}_i$ is the force acting on $\boldsymbol{r}_i$, tilde operator ($\tilde{\ }$) creates a tilde matrix (a skew-symmetric matrix), and prime ($'$) indicates that those variables with prime are shown on the body coordinate system. We choose a Lyapunov function to give

$$V = \frac{1}{2}\boldsymbol{\omega}^{\top}\boldsymbol{J\omega}. \tag{3}$$

From this equation onwards, we omit to writing $'$ (prime). The time derivative of V becomes

$$\dot{V} = \boldsymbol{\omega}^{\top}\boldsymbol{J\dot{\omega}}$$

$$= \boldsymbol{\omega}^{\top}\left(\boldsymbol{\tilde{r}}_i\boldsymbol{f}_i - \boldsymbol{\tilde{\omega}J\omega}\right). \tag{4}$$

The force $\boldsymbol{f}_i(= [f_{ix}, f_{yi}, f_{iz}]^{\top})$ contains the force from the spring-damper of the landing gear $\boldsymbol{f}_{Si}$ and the constraining force acts on the linear restriction between the lander main body and the landing leg $\boldsymbol{f}_{Ri}$, as follows:

$$\boldsymbol{f}_i = \boldsymbol{f}_{Si} + \boldsymbol{f}_{Ri}. \tag{5}$$

Assigning this to equation(4):

$$\dot{V} = \boldsymbol{\omega}^{\top}\left\{\boldsymbol{\tilde{r}}_i\left(\boldsymbol{f}_{Si} + \boldsymbol{f}_{Ri}\right) - \boldsymbol{\tilde{\omega}J\omega}\right\}. \tag{6}$$

In this equation, only $\boldsymbol{f}_{Si}$ can be controlled by changing the damping coefficient c_i. Thus, to minimize the time derivative of the Lyapunov function, only the term related to $\boldsymbol{f}_{Si}$ should be considered, as follows:

$$\dot{V}_{Si} = \boldsymbol{\omega}^{\top}\left(\boldsymbol{\tilde{r}}_i\boldsymbol{f}_{Si} - \boldsymbol{\tilde{\omega}J\omega}\right) \tag{7}$$

Upon expansion to matrix elements, $\dot{V}_{Si}$ is written as,

$$\dot{V}_{Si} = \begin{bmatrix} \omega_x & \omega_y & \omega_z \end{bmatrix} \left(\begin{bmatrix} r_{ix} \\ r_{iy} \\ r_{iz} \end{bmatrix} \times \begin{bmatrix} f_{Six} \\ f_{Siy} \\ f_{Siz} \end{bmatrix} - \begin{bmatrix} \omega_x \\ \omega_y \\ \omega_z \end{bmatrix} \times \begin{bmatrix} J_x & & \\ & J_y & \\ & & J_z \end{bmatrix} \begin{bmatrix} \omega_x \\ \omega_y \\ \omega_z \end{bmatrix} \right) \tag{8}$$
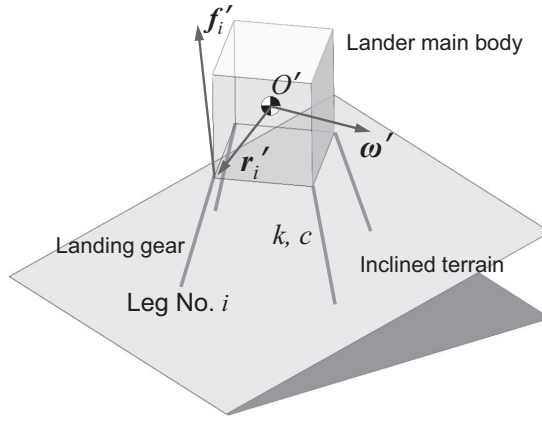
Fig. 3 Three-dimensional lander touchdown model

The body is symmetrical about the $x-z$ and $y-z$ planes, such that the moment of inertia $J_x = J_y = J_t$ and $J_z = J_s$. Here, $\boldsymbol{r}_i$ and $\boldsymbol{f}_{Si}$ are provided in the same plane which is perpendicular to the $x-y$ plane of the lander coordinates. Thus the third component of the outer product of $\boldsymbol{r}_i$ and $\boldsymbol{f}_{Si}$ is equal to zero. Based on these assumptions, $\dot{V}_{Si}$ is written as,

$$\dot{V}_{Si} = \begin{bmatrix} \omega_x & \omega_y & \omega_z \end{bmatrix} \left(\begin{bmatrix} r_{iy}f_{iz} - r_{iz}f_{iy} \\ r_{iz}f_{ix} - r_{ix}f_{iz} \\ 0 \end{bmatrix} - \begin{bmatrix} \omega_y\omega_z(J_s - J_t) \\ \omega_x\omega_z(J_t - J_s) \\ 0 \end{bmatrix} \right)$$
$$= \omega_x \left(r_{iy}f_{iz} - r_{iz}f_{iy} \right) + \omega_y \left(r_{iz}f_{ix} - r_{ix}f_{iz} \right). \tag{9}$$

The force acting on the landing leg $\boldsymbol{f}_{Si}$ shown in Figure 4 can be described by the direction of the linear motion of the landing leg $\boldsymbol{r}_{Si}$ and the size of force f_{Si} like Figure 5, as follows:

$$\boldsymbol{f}_{Si} = f_{Si}\boldsymbol{r}_{Si}. \tag{10}$$

Here, the direction $\boldsymbol{r}_{Si}$ can described by $\boldsymbol{r}_i$ and constant coefficient β and γ. The x, y and z components of $\boldsymbol{r}_{Si}$ are described as,

$$r_{Six} = -\beta r_{ix}, \quad r_{Siy} = -\beta r_{iy}, \quad r_{Siz} = -\gamma r_{iz}. \tag{11}$$
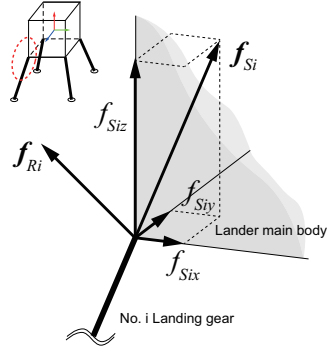
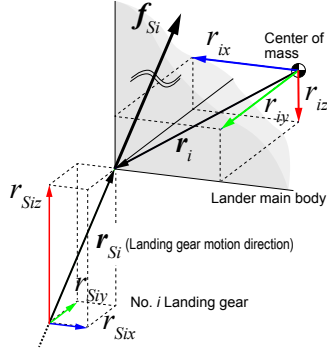Fig. 4 Force distribution in the direction of the local coordinate of the landing gear

Fig. 5 Force and landing gear direction and installed point of landing gear relationships

where β and γ are described by the components of $\boldsymbol{r}_i$ and $\boldsymbol{r}_{Si}$, as follows:

$$\beta_i = \frac{\sqrt{r_{Six}^2 + r_{Siy}^2}}{\sqrt{r_{ix}^2 + r_{iy}^2}} \tag{12}$$

$$\gamma_i = - r_{Siz}/r_{iz} \tag{13}$$

We assumed that the lander was symmetrical. Therefore, all the legs have the same value of β_i and γ_i. The landing gear is usually installed nearly vertical; thus, the absolute value of β becomes smaller than that of γ. Hence, the equation (9) becomes,

$$\dot{V}_{Si} = f r_{iz}(-\gamma + \beta)\left(\omega_x r_{iy} - \omega_y r_{ix}\right). \tag{14}$$

Here, if the sign of r_{iz} is negative, the sign of γ is positive, then the sign of $(-\gamma + \beta)$ must be negative. On the other hand, the sign of r_{iz} is positive, the sign of γ is negative, then, the sign of $(-\gamma + \beta)$ must be positive. Therefore, the sign of $r_{iz} \times (-\gamma + \beta)$ is always positive. Based thereupon,

the derivative of Lyapunov function is as follows:

$$\dot{V}_{Si} = f_{Si}\alpha\left(\omega_x r_{iy} - \omega_y r_{ix}\right),\tag{15}$$

where α is positive constant.

The force f_{Si} is as follows:

$$f_{Si} = -c_i \dot{d}_i - k d_i,\tag{16}$$

where c_i is a damping coefficient, k is a spring coefficient and d_i and $\dot{d}_i$ are the displacement and velocity of the spring-damper. d_i is positive in the direction to extend the length of spring-damper. If we assign f_{Si} to equation (15), then

$$\dot{V}_{Si} = -\alpha\left(c_i \dot{d}_i + k d_i\right)\left(-\omega_y r_{ix} + \omega_x r_{iy}\right).\tag{17}$$

To consider a landing gear with multiple legs, the time derivative of the Lyapunov function is as shown below:

$$\dot{V}_{\text{all}} = -\sum_{i=1}^{N} \alpha\left(c_i \dot{d}_i + k d_i\right)\left(-\omega_y r_{ix} + \omega_x r_{iy}\right),\tag{18}$$

where N is the number of landing gear legs. We assumed that only the damping coefficient c_i is controllable. Therefore, the convergence time of the angular velocity of the lander can be shortened by choosing each damping coefficient c_i from $c_{\min}$ and $c_{\max}$ to minimize the time derivative of the Lyapunov function $\dot{V}_{\text{all}}$, moment by moment. To achieve this, the damping coefficient c_i is determined from the next formula,

$$c_i = \frac{c_{\max} - c_{\min}}{2}\, \text{sgn}\left[(-\omega_y r_{ix} + \omega_x r_{iy})\dot{d}_i\right] + \frac{c_{\max} + c_{\min}}{2}.\tag{19}$$

IV.   Landing simulation for four-legged lander

A.   Overview of landing simulation

We conducted numerical simulations of the landing sequence to evaluate the effectiveness of the control systems. The simulation model is shown in Figure 6 while the corresponding parameters are listed in Table 1. This model has multiple ($N = 4$) landing legs. The motion of each landing leg is limited to linear motion relative to the initial state. The moment of inertia of the landing legs is ignored to simplify the equation of motion.

The lander size is decided by referring to the size of the SLIM lander that has been designed by the Japan Aerospace Exploration Agency (JAXA) for a Moon landing [14]. The lander parameters are listed in Table 1. We assume that the main body and the landing gear are rigid. Flexibility is not considered. The main body of the lander is defined as a rigid body. The landing gear is defined as a mass point and is attached to the body through a spring and a damper. Its motion is restricted to linear motion.

Here, we explain the method used to determine landing gear parameters k and c. First, we decide the damping ratio and the nominal displacement d_{nom} of the landing gear when the lander touches down on a horizontal smooth surface. Here, we select a damping ratio ζ such that its value is 1.0 (critical damping) when the lander touches down with all the legs of the landing gear. The nominal displacement is 0.2 m. Second, based on these parameters, the nominal stiffness k_{nom} and the nominal damping coefficient c_{nom} were determined. Third, we assume that the variable damper can change its damping coefficient from c_{min} to c_{max}. The dynamic range of the variable damper depends on the type of energy dissipation and design. It seems possible to design with a 5 to 10 times dynamic range damper by using magnetorheological fluid, according to documents in reference[15, 16]. For example, typical MR damper LORD-RD-8041[17] which shown in Figure 2 can change the damping force within a range of 10 times. Thus, we assume that the damper can change its damping coefficient from c_{min} to c_{max} with a 10 times dynamic range in the following simulations.

It is assumed that the terrain surface is rigid and akin to bedrock. As the stiffness of the terrain increases, less energy is dissipated into the surface. Thus, sufficiently large and small values are used for the stiffness k_T and damping coefficient c_T, respectively, between the terrain and footpad.

The coefficient of friction between the footpad and terrain μ' is around 0.7, based on the data obtained by NASA's Surveyor lander[18]. Our previous research determined that it would be more difficult to achieve touchdown without tip-over when the friction is large[13]. Therefore, the dynamic friction coefficient between the footpad and the terrain was set to a value of 1.0, which is larger than we would expect.

The equation of motion is expressed as a differential algebraic equation that incorporates a
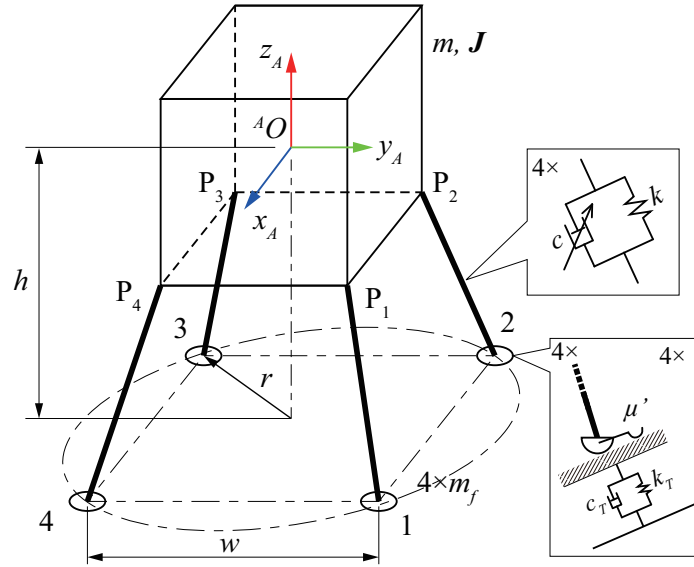
Fig. 6 Overview of 3-D lander simulation model (four-leg case)

Table 1 Lander 3-D model parameters.

	Parameter	Value	Unit
N	Number of landing legs	3-20	-
m	Mass of body	130	kg
$\boldsymbol{J}$	Moment of Inertia (x, y, z)	$[20, 20, 25]$	kgm^2
m_f	Mass of each landing leg	$20/N$	kg
w	Total width	1.2	m
r	Radius of footpad circle	$1.2/\sqrt{2}$	m
h	Lander center of mass height	1.2	m
k	Spring constant	$4.0/N$	kN/m
c_{nom}	Nominal damping coefficient	1.4 (for passive leg)	kNs/m
c_i	Damping coefficient (variable)	$0.3c_{\text{nom}}$-$3.0c_{\text{nom}}$	kNs/m
k_T	Spring constant of soil surface	100	kN/m
c_T	Damper constant of soil surface	0.10	kNs/m
μ'	Terrain dynamic friction	1.0	-
H	Initial height of center of gravity of the body	3.5	m

restriction equation. The constraining force is represented by Lagrange's undetermined multipliers.

The equation of motion is as follows[19],

$$
\begin{bmatrix} \boldsymbol{M} & \boldsymbol{0} & \boldsymbol{\Phi}_v^\top \\ \boldsymbol{0} & \boldsymbol{J}' & \boldsymbol{\Phi}_{\omega'}^\top \\ \boldsymbol{\Phi}_v & \boldsymbol{\Phi}_{\omega'} & \boldsymbol{0} \end{bmatrix} \begin{bmatrix} \dot{\boldsymbol{v}} \\ \dot{\boldsymbol{\omega}}' \\ \boldsymbol{\lambda} \end{bmatrix} = \begin{bmatrix} \boldsymbol{f} \\ \boldsymbol{\tau}' - \tilde{\boldsymbol{\omega}}' \boldsymbol{J}' \boldsymbol{\omega}' \\ -\dot{\boldsymbol{\Phi}}_{\overline{v\omega'}} \end{bmatrix} \tag{20}
$$

where, $\boldsymbol{M}$ is the mass matrix, $\boldsymbol{J}$ is matrix for the moment of inertia as follows:

$$
\boldsymbol{M} = \mathrm{diag}\,(m, m, m,\ m_f, m_f, m_f, \ldots, m_f, m_f, m_f) \tag{21}
$$

$$
\boldsymbol{J} = \mathrm{diag}\,(J_x, J_y, J_z) \tag{22}
$$

The moment of inertia of the footpad is omitted because the footpad is defined as being a mass point. $\boldsymbol{v}$ is the velocity vector, $\boldsymbol{\omega}'$ is the angular velocity vector, $\boldsymbol{f}$ is the force vector, $\boldsymbol{\tau}$ is the torque vector, $\boldsymbol{\Phi}$ is the constraint equation. And $\boldsymbol{\Phi}_v$ and $\boldsymbol{\Phi}_{\omega'}$ are partially differentiated by translational velocity $\boldsymbol{v}$ and angular velocity $\boldsymbol{\omega}'$. $\dot{\boldsymbol{\Phi}}_{\overline{v\omega'}}$ is the residual part of the time derivative of the constraint condition that is not related to the time derivative of either $\boldsymbol{v}$ or $\boldsymbol{\omega}'$. The prime ($'$) means that the vector is shown on the body coordinate system.

The constraint condition of the landing gear is shown in Figure 7. $\boldsymbol{R}_{\mathrm{body}}$, $\boldsymbol{R}_{Fi}$, and $\boldsymbol{R}_{Pi}$ are the vectors from the origin of the global coordinates to the center of gravity of the body, footpad, and the mounting position of the landing gear, respectively. $\boldsymbol{r}_i$ is a vector from the center of gravity of the lander body to the mounting position of the landing gear. $\boldsymbol{s}_i$ is a vector from the landing gear lower part to the point at which the landing gear mounts to the body, and $\boldsymbol{r}_{Si\mathrm{INIT}}$ is a vector of the initial direction of the landing gear which is fixed to the body coordinates. $\boldsymbol{n}_{ai}$ and $\boldsymbol{n}_{bi}$ are the vectors perpendicular to the initial direction of motion of the landing gear $\boldsymbol{r}_{Si\mathrm{INIT}}$. They are calculated by $\boldsymbol{r}_{Si\mathrm{INIT}}$, and they are also fixed to the body coordinates. Both vectors, $\boldsymbol{n}_{ai}$, $\boldsymbol{n}_{bi}$ are orthogonal to each other. If the vector of the current direction of motion $\boldsymbol{s}_i$ and that of the initial direction $\boldsymbol{r}_{Si\mathrm{INIT}}$ exist on the same line, the constraint condition for telescopic motion is satisfied. To satisfy this requirement, $\boldsymbol{s}_i \perp \boldsymbol{n}_{ai}$ and $\boldsymbol{s}_i \perp \boldsymbol{n}_{bi}$ are required. Thus, it is necessary to satisfy the following equation.

$$
\boldsymbol{n}_{(a,b)i}^\top \boldsymbol{s}_i = 0 \tag{23}
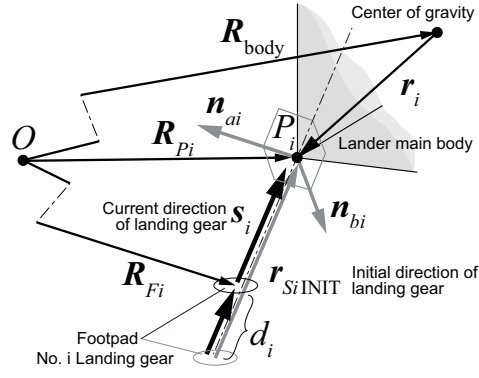$$

13

Fig. 7 Vector of direction of motion of landing gear for constraint condition
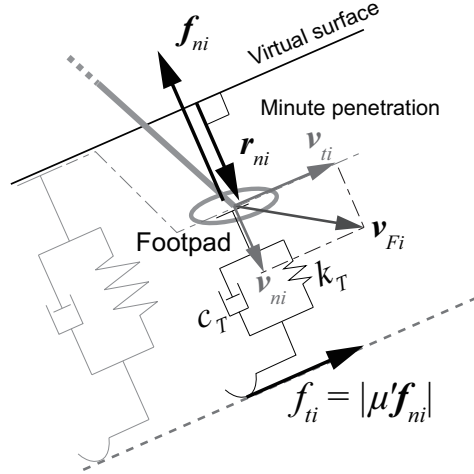
Fig. 8 Footpad terrain contact model

Therefore, the equation of constraint is as follows,

$$\boldsymbol{\Phi} = \left[\boldsymbol{s}_1^\top \boldsymbol{n}_{a1}, \ldots, \boldsymbol{s}_4^\top \boldsymbol{n}_{a4}, \ \boldsymbol{s}_1^\top \boldsymbol{n}_{b1}, \ldots, \boldsymbol{s}_4^\top \boldsymbol{n}_{b4} \right]^\top. \tag{24}$$

The force acting on the main body from the landing gear $\boldsymbol{f}_{Si}$ is obtained as follows,

$$\boldsymbol{f}_{Si} = (-kd_i - c\dot{d}_i)\frac{\boldsymbol{s}_i}{|\boldsymbol{s}_i|}. \tag{25}$$

The terrain model is shown in Figure 8. The force acting on the footpad $\boldsymbol{f}_{Fi}$ is obtained from the penetration $\boldsymbol{r}_{ni}$ and the velocity of the footpad $\boldsymbol{v}_{Fi}$. The normal force $\boldsymbol{f}_{ni}$, tangential force $\boldsymbol{f}_{ti}$, and

14

total force $\boldsymbol{f}_{Fi}$ are as follows:

$$\boldsymbol{f}_{ni} = -k_T \boldsymbol{r}_{ni} - c_T \boldsymbol{v}_{ni} \tag{26}$$

$$\boldsymbol{f}_{ti} = -|\mu' \boldsymbol{f}_{ni}| \frac{\boldsymbol{v}_{ti}}{|\boldsymbol{v}_{ti}|} \tag{27}$$

$$\boldsymbol{f}_{Fi} = \boldsymbol{f}_{ni} + \boldsymbol{f}_{ti} \tag{28}$$

Therefore, the force $\boldsymbol{f}$ and torque $\boldsymbol{\tau}$ in equation (20) are equal to

$$\boldsymbol{f} = \left[\sum_{i=1}^{4} \boldsymbol{f}_{Si} + m\boldsymbol{g}; -\boldsymbol{f}_{S1} + \boldsymbol{f}_{F1} + m_f \boldsymbol{g}; \ldots; -\boldsymbol{f}_{S4} + \boldsymbol{f}_{F4} + m_f \boldsymbol{g} \right] \tag{29}$$

$$\boldsymbol{\tau} = \left[\sum_{i=1}^{4} (\tilde{r}_i \boldsymbol{f}_{Si}) \right] \tag{30}$$

The differential algebraic equation (20) was numerically solved by application of the 4th-order Runge-Kutta method, and the simulation was carried out using MATLAB R2015a.

B. Landing on inclined terrain

The effectiveness of the control method for the variable-damping landing gear was verified by performing a touchdown simulation. Here, we focus on a touchdown on inclined terrain that constitutes the most dangerous situation that a lander is likely to encounter. To validate the anti-falling ability of the variable damping shock absorber of the landing gear, first, the touchdown simulations on an inclined terrain with and without variable damper are shown. Second, the relationship between the anti-falling ability and the numbers of landing legs is described.

Figures 9 and 10 show the results of a simulation of a touchdown on a slope with an angle of $\phi = 20°$. Figure 9 shows the case in which the angle between the lander and the direction of the slope ψ is $45°$ (2-2 contact) and Figure 10 shows the case for $\psi = 25°$ (1-1-1-1 contact). In these figures, a) and c) show the overview of the simulation, b) and d) show the time-series history of the angle of the lander θ, e) and g) show the time-series history of the forces acting on each landing leg, and f) and h) show the time-series history of the displacement and speed of the landing gear shock absorber. Here, the a), b), e), and f) results are obtained without a variable damper (passive), while the c), d), g), and h) results are obtained with a variable damper (semi-active). Finally, i) shows the history of the variable damper's damping coefficient.

Here, we focus on the force acting on each landing leg. A large force acting on the two higher legs ($i = 1, 4$) causes tripping. On the other hand, a large force acting on the two lower legs ($i = 2, 3$) prevents overturning. The case without a variable damper, with a large force acting on the upper legs and a small force acting on the lower legs, is shown in Figure 9(e). The variable damper reduces the force acting on the upper legs and increases the force acting on the lower legs, as shown in Figure 9(g). Thus, the switching of the damping coefficient as shown in Figure 9(g) is effective. This controller sets the damping coefficient automatically based on the lander attitude and the direction of the displacement rate of each landing leg. Here, the damping coefficient of the two upper legs is reduced after making contact with the surface and increased after the two lower legs make contact. The damping coefficient of the two lower legs is first reduced and increased after making contact with the surface. As a result, tripping is prevented.

In Figure 9(g), The peak forces acting on the lower legs ($i = 2, 3$) become larger than those

16

shown in Figure 9(e) ($i = 1, 4$). This is caused by an increase in the damping coefficient. The controller increases the damping coefficient from the nominal value such that the damping force increases. The peak force is determined by the initial speed of contact between the landing gear and the terrain. An increase in the damping coefficient leads to an increase in the damping force acting on the landing gear. Therefore, a large force spike appears in the results obtained with control. Our focus was not on the mitigation of acceleration, however, but on the prevention of overturning. Hence, this spike force is acceptable because it prevents the tipping-over of the lander.

Next, we focus on the displacement of the landing gear at touchdown. The displacement of the upper legs when fitted with a variable damper is larger than in the case when there is a fixed damper. On the other hand, the displacement of the lower legs is smaller when the variable damper is fitted. This situation is conducive to the prevention of tip-over. Due to the aforementioned reasons, the switching of the damping coefficient as shown in Figure 9(i) is effective.

Figure 10 shows the results of a twisted touchdown with an angle of twist of $\psi = 25°$ with respect to the direction of the inclination. We can draw the same conclusions about this case as for the case when $\psi = 45°$. The timing at which the leg makes contact differs from the case when $\psi = 45°$. When $\psi = 45°$, the legs make contact with the surface in the order of 1,4-2,3. When $\psi = 25°$, however, the legs make contact with the surface in the order of 1-4-2-3. In this case, the variable damper can also prevent tripping. Especially, when the twist angle $\psi \neq 45°$ or $\psi \neq 0°$, rotational motion arises not only in the direction of the inclination (pitch motion) but also in the direction of the contour line (roll motion). The proposed controller can also suppress this directional rotation. The forces and control inputs that prevent rotation in the direction of the contour line are shown in Figures 10(g) and (i). The control input for the legs that make contact with the surface first ($i = 1$) and last ($i = 3$), exhibit a history that is similar to the case of $\psi = 45°$. However, for the second and third legs to make contact with the surface ($i = 4, 2$), the control inputs fluctuate intensely around the moment of contact. This causes short peaks in the force acting on the No. 4 leg (f_{S4}), which prevents the rotation of the lander. Regarding the displacement of the landing gear, relative to the passive case, the uppermost leg ($i = 1$) exhibited increased displacement, while the displacement of the lowest leg ($i = 3$) decreased when a variable damper was fitted.
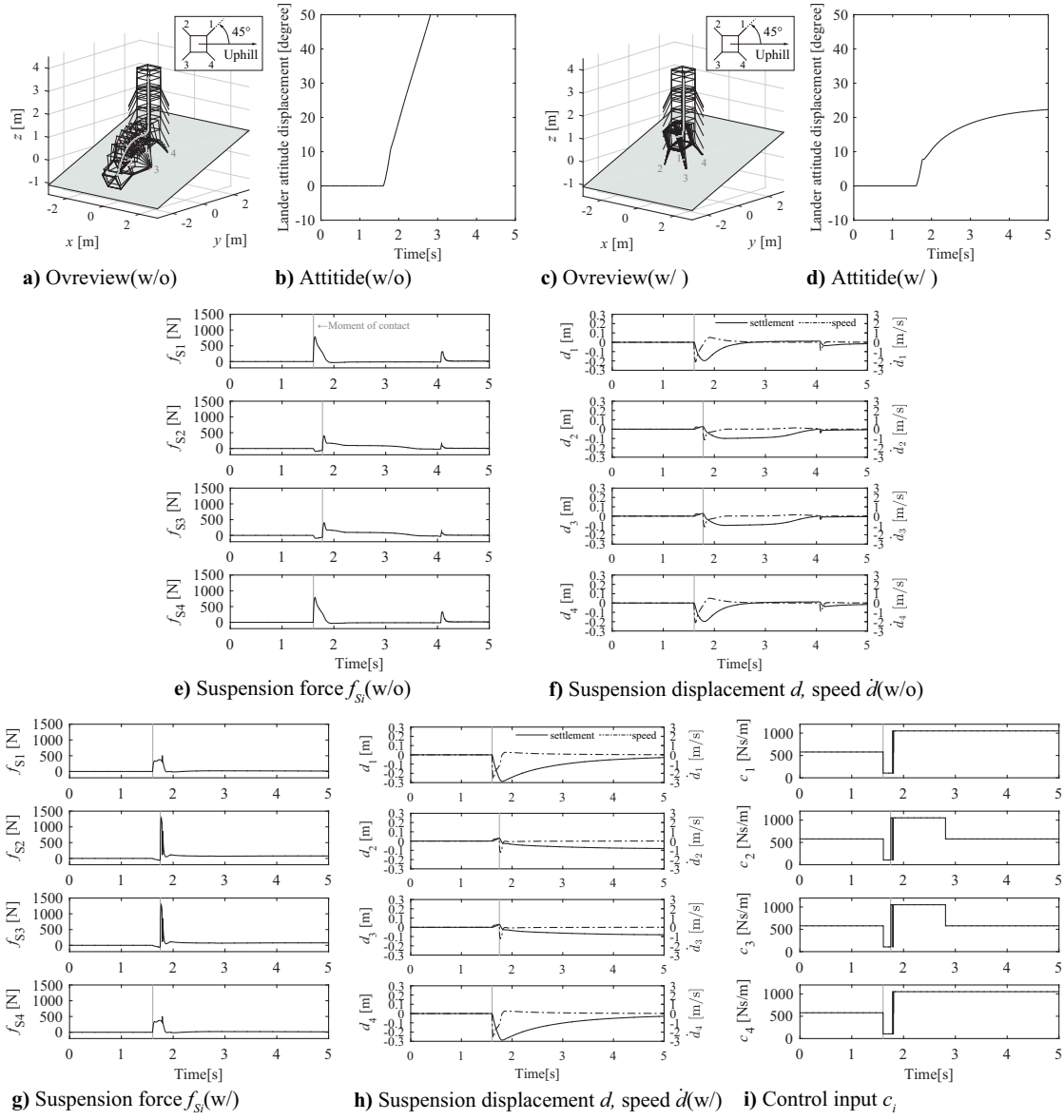
17

a) Ovreview(w/o) **b)** Attitide(w/o) **c)** Ovreview(w/) **d)** Attitide(w/)

e) Suspension force f_{Si}(w/o) **f)** Suspension displacement d, speed $\dot{d}$(w/o)

g) Suspension force f_{Si}(w/) **h)** Suspension displacement d, speed $\dot{d}$(w/) **i)** Control input c_i

Fig. 9 Comparison of the attitude and the force between passive and variable landing gear and control input. (no.1,4-2,3 contact, $\phi = 20°$, $\psi = 45°$)

According to the above results, the proposed controller would also be effective in the event of a landing with a twist, with respect to the direction of the inclination.
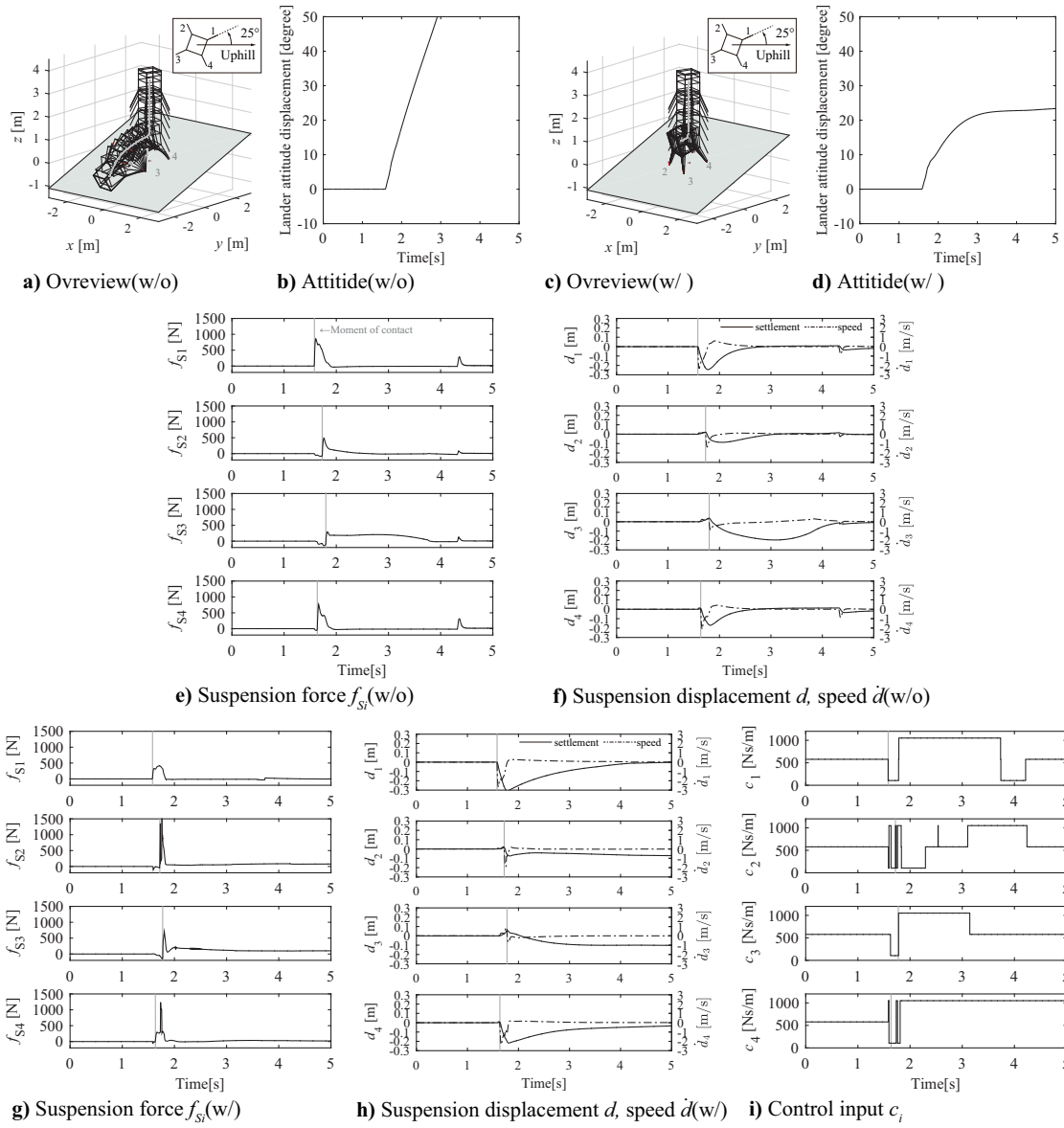
a) Ovreview(w/o) **b)** Attitide(w/o) **c)** Ovreview(w/) **d)** Attitide(w/)

e) Suspension force f_{Si}(w/o) **f)** Suspension displacement d, speed $\dot{d}$(w/o)

g) Suspension force f_{Si}(w/) **h)** Suspension displacement d, speed $\dot{d}$(w/) **i)** Control input c_i

Fig. 10 Comparison of attitude and force between passive and variable landing gear and control input. (no.1-4-2-3 contact, $\phi = 20°$, $\psi = 25°$)

C. Landing with lateral velocity

Next, we focused on a touchdown with a lateral velocity that also gives rise to a serious risk of the lander overturning. In the case of a touchdown with lateral velocity, the friction between the footpad and the terrain causes torque that rotates the lander body in the direction of travel. In this case, the lander could topple by rotating around the points at which the front legs make contact with the surface. If the vertical force that acts on each landing leg were to be controllable, it would be possible to generate an anti-rolling torque by using the difference in the forces between the front and rear legs. A controller based on formula (19) could satisfy this requirement. To validate the anti-tripping ability, we performed a touchdown simulation with an initial velocity in a lateral direction.

Figures 11 and 12 show the results of the touchdown with an initial lateral velocity of 1.5 m/s. Figure 11 shows the case of a landing with an angle between the lander and the direction of the initial velocity ψ of 45°, while Figure 12 shows the case for $\psi = 25°$.

In each of these figures, a) and c) show the simulation, b) and d) show the time-series histories of the angle of the lander θ, e) and g) are the time-series histories of the forces acting on each landing leg, and f) and h) are the time-series histories of the displacement and speed of the landing gear shock absorber. Here, a), b), e), and f) show the results without a variable damper (passive) and c), d), g), and h) show the results obtained with a variable (semi-active) damper. Finally, i) shows the history of the variable damper's damping coefficient.

Here, we also focus on the force acting on each landing leg. The causes of the tipping are the force acting on the rear leg and the large displacement of the front leg. The large force acts on the front legs in the normal direction to the surface to prevent tripping.

Regarding the displacement of the landing leg, the displacement of the front damper ($i = 1, 4$) of the active case is smaller than that in the passive case. This also contributes to the prevention of overturning.

The simulation result in the case of a twist angle ψ is 45° as shown in Figure 11. Without a variable damper, the large force acts on the front legs ($i = 1, 4$) as shown in Figure 11(e). In contrast, the variable damper reduces the force acting on the front legs, as shown in Figure 11(g) by

changing the damping coefficient as shown in Figure 11(i) by using the same controller as that used for landing on the incline. The force acting on the front legs increases to prevent overturning. The effectiveness of the controller that sets the damping coefficient is automatically based on the lander angular velocity and the direction of the displacement rate of each landing leg is certified by those simulations. Here, the damping coefficient input for the front legs is increased after contact with the surface and then decreased soon after. The first high input of the damping coefficient produces a large force on the front leg, which prevents tipping. The decreasing damping coefficient after the first high input has the effect of suppressing vibration in the lander.

When $\psi = 25°$, the order in which the landing gear legs touch down from the velocity direction is 1-4-2-3. The force acting on the front legs ($i = 1, 4$) with the variable damper shown in Figure 12(f) becomes larger than the force with the passive shown in Figure 12(g). The input of the damping coefficient of the most front side leg ($i = 1$) set large after contact and this prevents overturning. The input to the second front leg ($i = 4$) also becomes large, but soon becomes small again. This result has an effect of roll attitude stabilization.

a) Ovreview(w/o) **b)** Attitide(w/o) **c)** Ovreview(w/) **d)** Attitide(w/)

e) Suspension force f_{Si}(w/o) **f)** Suspension displacement d, speed $\dot{d}$(w/o)

g) Suspension force f_{Si}(w/) **h)** Suspension displacement d, speed $\dot{d}$(w/) **i)** Control input c_i
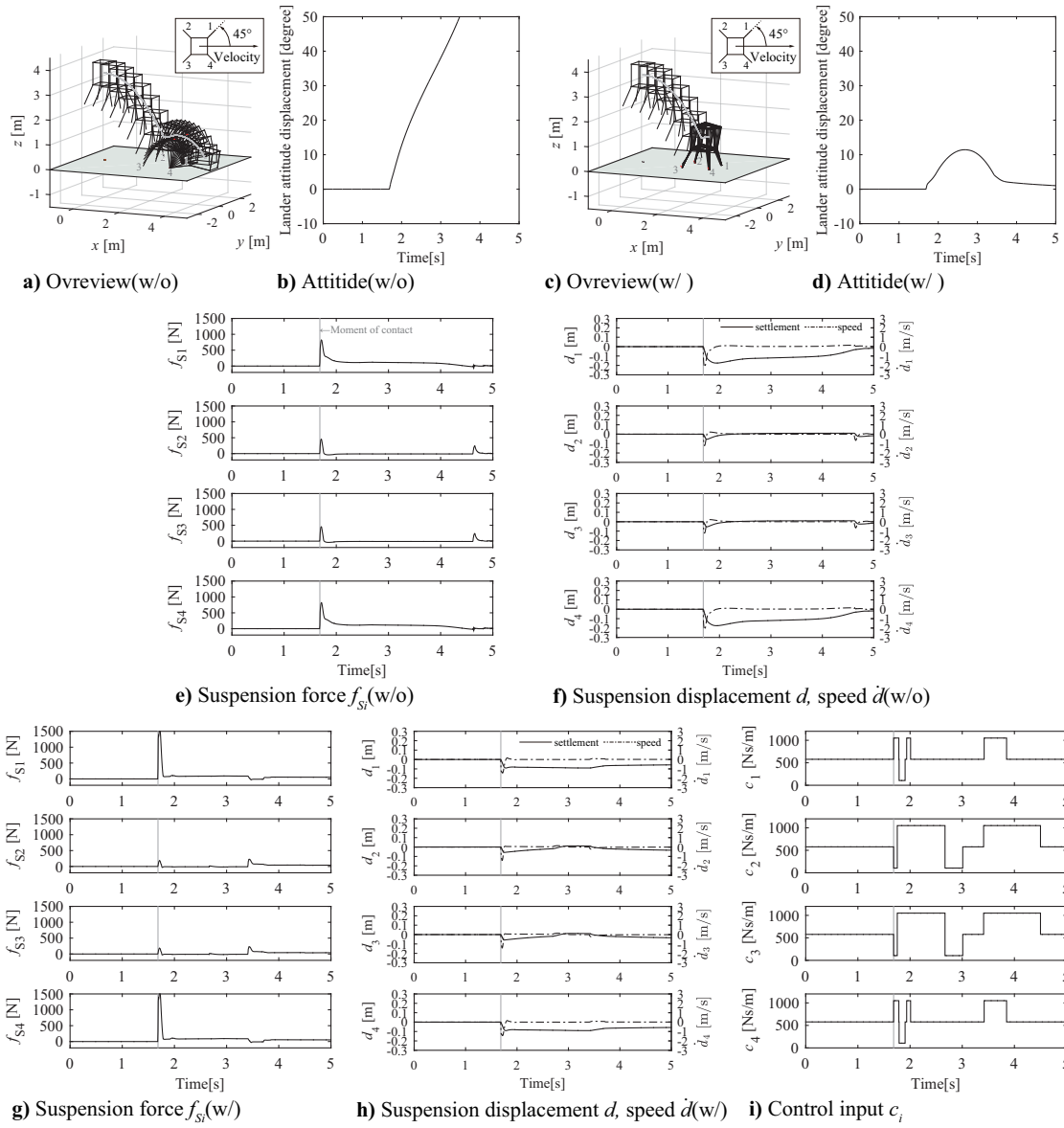
Fig. 11 Comparison of attitude and force between passive and variable landing gear and control input. (no. 1, 4 - no. 2, 3 contact, $v_x = 1.5$ [m/s], $\psi = 45°$)
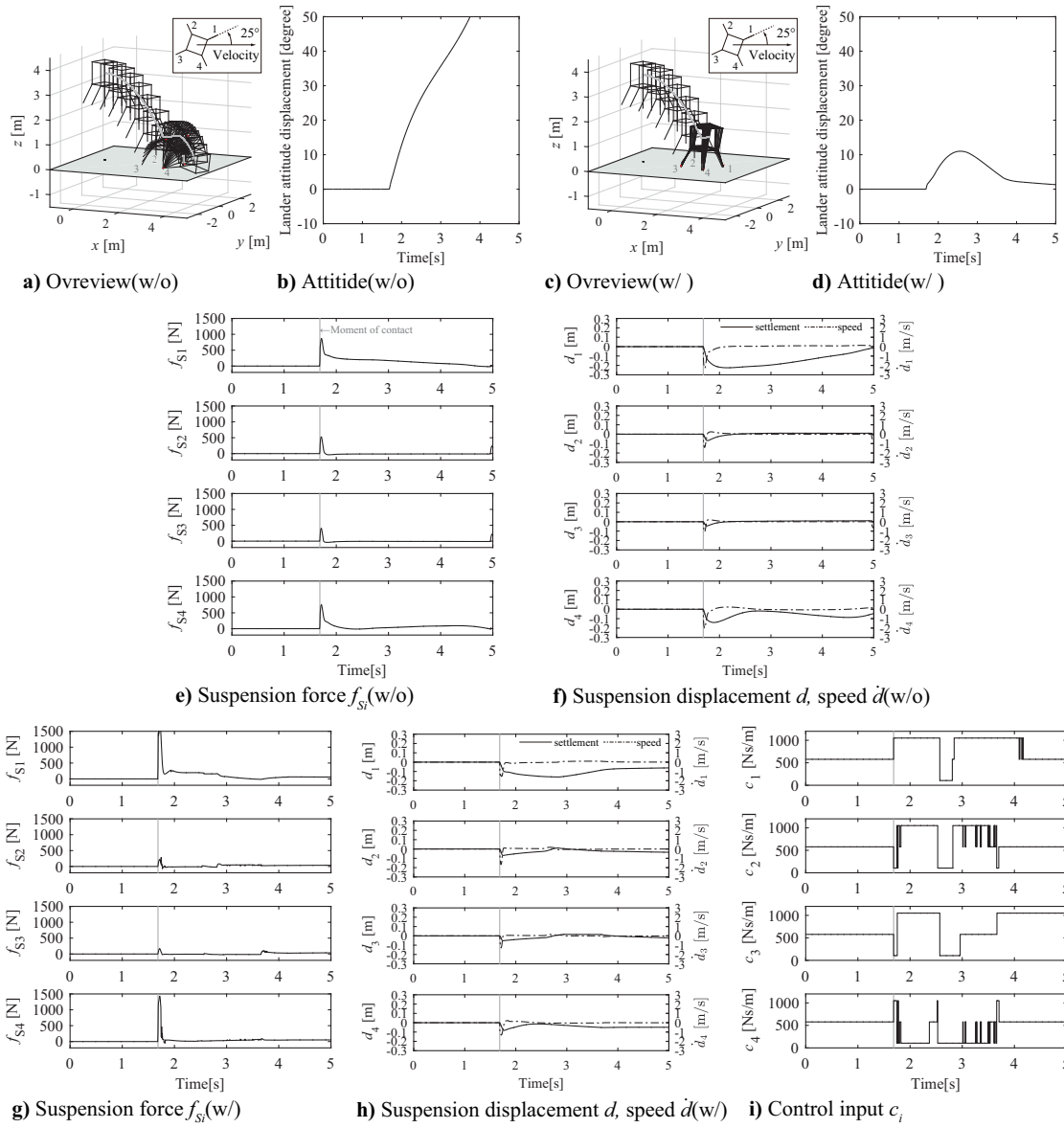
a) Ovreview(w/o)   **b)** Attitide(w/o)   **c)** Ovreview(w/)   **d)** Attitide(w/)

e) Suspension force f_{Si}(w/o)   **f)** Suspension displacement d, speed $\dot{d}$(w/o)

g) Suspension force f_{Si}(w/)   **h)** Suspension displacement d, speed $\dot{d}$(w/)   **i)** Control input c_i

Fig. 12 Comparison of attitude and force between passive and variable landing gear and control input. (no. 1 - 4 - 2 - 3 contact, $v_x = 1.5$ [m/s], $\psi = 25°$)

D. Landing with translation- and rotation-coupled dynamics

In this section, we address a touchdown on an inclined terrain with a lateral velocity. In this case, the lander touches the inclined terrain with a lateral velocity. There are many possible combinations of direction of incline and velocity. Here, one embodiment of the simulation is shown to confirm the validity of the proposed variable damping landing gear.

Figures 13 and 14 show the results of the touchdown with an initial lateral velocity of 1.5 m/s on a slope with an angle of $\phi = 15°$. Figure 13 shows the case of a landing with an angle between the lander and the direction of the initial velocity ψ of 45°, while Figure 14 shows the case for $\psi = 25°$. The angle between the direction of the lateral velocity and the direction of the incline is equal to 90°.

In each of these figures, a) and c) show the overview, b) and d) show the time-series history of the angle of the lander θ, e) and g) are the time-series history of the forces acting on each landing leg, and f) and h) are the time-series history of the displacement and speed of the landing gear shock absorber. Here, a), b), e), and f) show the results obtained without a variable damper (passive), while c), d), g), and h) show the results obtained with a variable damper (semi-active). Finally, i) shows the history of the variable damper's damping coefficient.

Figure 13 (e) and (g) show that a force peak acting on the front legs ($i = 1, 4$) increases in the case with control. This force prevents the lander from tipping-over in the direction of translation. This is similar to the results obtained for touchdown with only a lateral velocity, as shown in Figure 11. Next, let us consider the displacement of the landing gear shown in Figure 13 (f) and (h). Without any control, the front-upper leg ($i = 1$) is the first to be compressed, but quickly re-assumes its normal length. The front-lower leg ($i = 4$) is also compressed considerably, leading to a rotational motion toward the valley side. On the other hand, with control, the front-upper leg ($i = 1$) is also considerably compressed, but it returns slowly. This is similar to the touchdown on inclined terrain shown in Figure 9. The history of displacement of the front-lower leg both without and with control is similar to that of the case of an incline, as shown in Figure 10. This leg acts almost as a lower leg because the lateral velocity is almost absorbed by two upper legs. Finally, let us consider the rear-lower leg ($i = 3$), which only moves a little. The attitude of the lander tilts
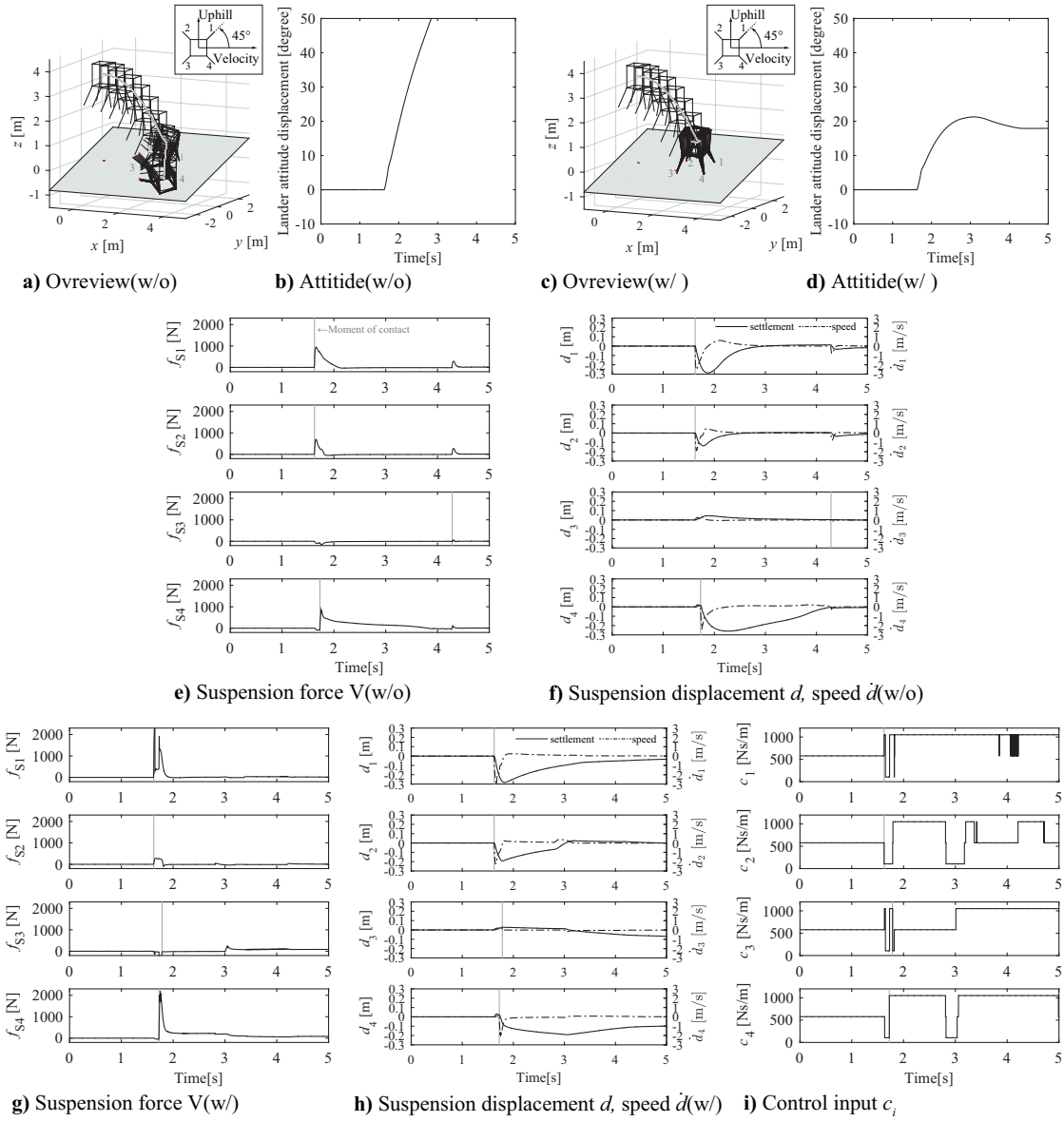
24

a) Ovreview(w/o)   **b)** Attitide(w/o)   **c)** Ovreview(w/)   **d)** Attitide(w/)

e) Suspension force V(w/o)   **f)** Suspension displacement d, speed $\dot{d}$(w/o)

g) Suspension force V(w/)   **h)** Suspension displacement d, speed $\dot{d}$(w/)   **i)** Control input c_i

Fig. 13 Comparison of attitude and force between passive and variable landing gear and control input. $(v_x = 1.5 \text{ [m/s]}, \phi = 15°, \psi = 45°)$

towards the front as a result of inertia, such that very little force acts on this leg.

The case of a touchdown with an angle of twist $\psi = 25°$ is shown in Figure 14. The result of the passive case tends to be similar to the case when $\psi = 45°$, as shown in Figure 13. The active case also tends to be similar to that of the case of $\psi = 45°$, as shown in Figure 13.

The above results indicate that the proposed controller for a semi-active landing gear is also effective when the lander exhibits translation-rotation coupled motion.
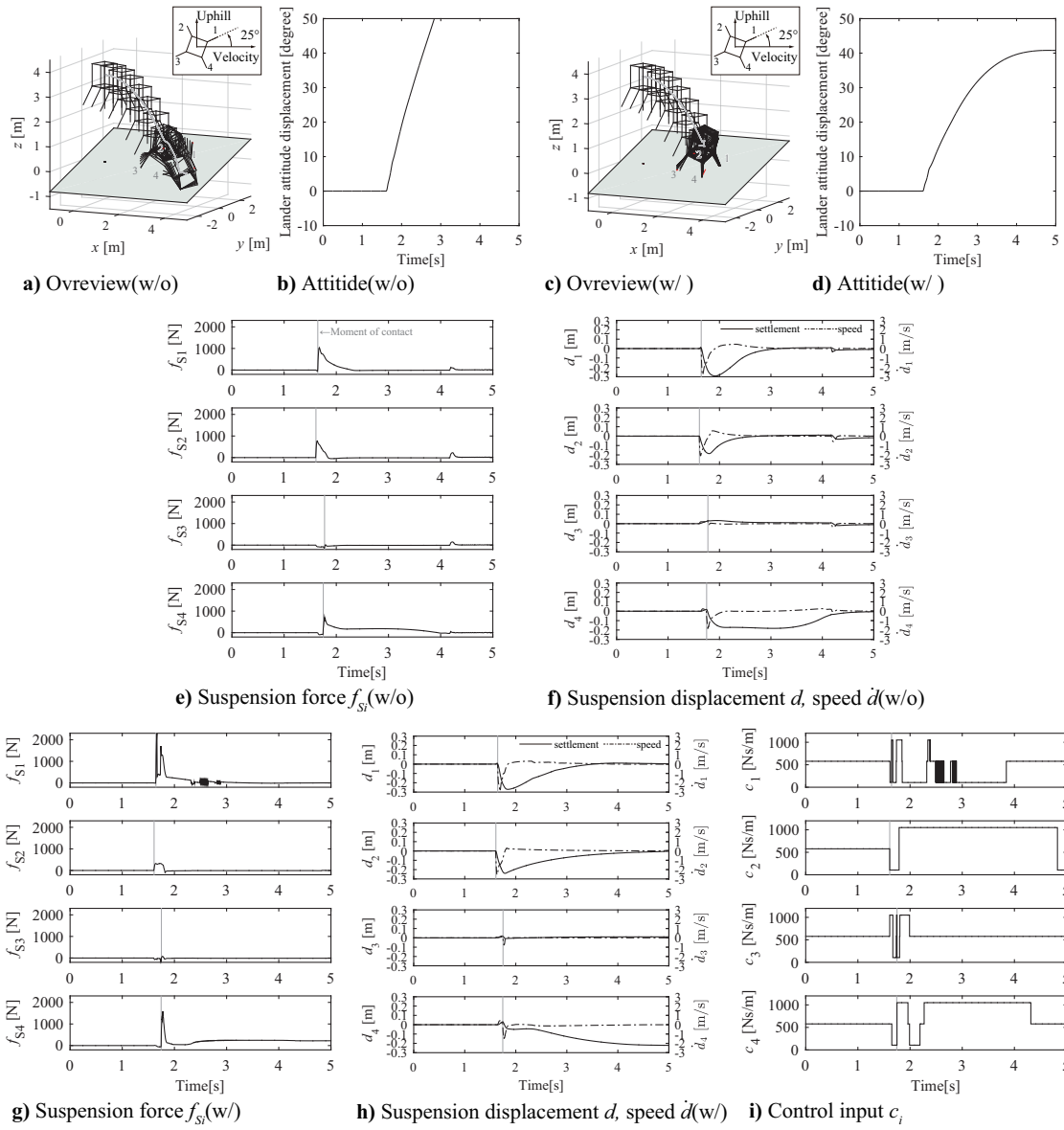
25

a) Ovreview(w/o) **b)** Attitide(w/o) **c)** Ovreview(w/) **d)** Attitide(w/)

e) Suspension force f_{Si}(w/o) **f)** Suspension displacement d, speed $\dot{d}$(w/o)

g) Suspension force f_{Si}(w/) **h)** Suspension displacement d, speed $\dot{d}$(w/) **i)** Control input c_i

Fig. 14 Comparison of attitude and force between passive and variable landing gear and control input. $(v_x = 1.5 \text{ [m/s]}, \phi = 15°, \psi = 25°)$

V. Relationship between number of legs and robustness against overturning

A. Overview of multiple landing leg simulation

Here, we investigate the relationship between the number of legs and the robustness against overturning. The maximum incline on which the lander can touch down without tripping depends on the number of landing legs. The overview of the lander with 3, 4, and 20 landing gears are shown in Figure 15. If the number of legs is increased, the area of the polygon for which the vertices are the toes of the landing legs becomes large. To attain static stability on the incline, this is effective. However, it is not enough to discuss the stability on the incline. In the 1960s, the relationship between the stability on an incline and the contact velocity was investigated by NASA for the Apollo lunar module [20, 21]. In that research, the effect of the twist angle (yaw angle) with respect to the direction of the incline was investigated by means of simulation and experiment and the likelihood of overturning to occur is shown. However, this contains only the result for a honeycomb crush shock absorber, while the lander shape also differs from our assumption. Therefore, we undertook a detailed simulation using the various types of landing gear with a multiple landing leg model. In particular, it is necessary to compare the performance of the variable damper with the passive damper. Therefore, we investigated the anti-overturning performance of a passive damper, variable damper, and honeycomb crush core.
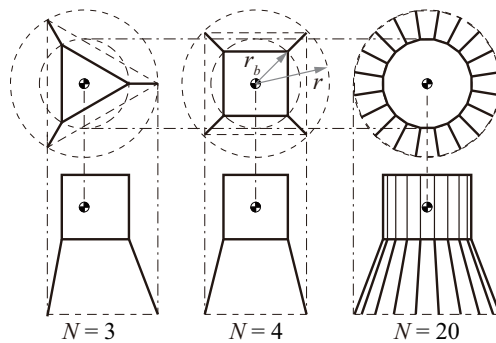

Fig. 15 Overview of the lander with 3, 4, and 20 landing gears.

B. Touchdown on inclined terrain

Figure 16 shows relationship between the maximum possible incline $\phi_{\max}$ of touchdown and the twist angle ψ with respect to the direction of the incline. The direction of a radius corresponds to the maximum inclination $\phi_{\max}$ while the circumferential direction refers to the twist angle ψ. Here, we define the angle between the no. 1 leg and the uphill direction of incline as being the twist ψ. The red line is the result for a landing gear without a variable damper (passive), the green line is the result for the honeycomb crush core, and the blue line is the result for the proposed variable damper. Here, the simulation results for three- to twenty-legged lander models are shown.

The results of the simulations show the efficacy of the variable damping landing gear with the proposed control method. The range of inclines on which a touchdown would be possible with the variable damping landing gear is superior those for the passive and the honeycomb landing gears, regardless of the number of landing legs. In the cases of the passive and honeycomb landing gears with three or four landing legs (Figure 16 a, b), the maximum inclination $\phi_{\max}$ depends on the angle between the lander and the direction of the slope ψ. In that case, $\phi_{\max}$ falls to a small value if the lander falls in a direction in which there are no legs. With the variable damper, $\phi_{\max}$ also becomes somewhat smaller in this direction, however, it is possible to land on an incline that is twice as steep as in the case with the passive and honeycomb landing gears.

There are two scenarios in which the application of the variable damper would prevent overturning. One is where the damping coefficient can be decreased to a lower than the nominal value. This reduces the force that acts in the direction to that in which the rolling of the lander body accelerates on the upper legs. The other is where the damping coefficient can be increased to a higher than the nominal value. This increases the force that acts in the direction to prevent rolling on the lower legs. The difference between the maximum and the minimum values of $\phi_{\max}$ for every case of ψ for the variable damper is smaller than that for the passive and honeycomb cases. This effect is a result of making the damping coefficient large and small. The initial impact acts on the upper legs, thus accelerating the rotating motion in the downhill direction, such that a small damping coefficient is better for reducing the force of the terrain acting on the lander main body. On the other hand, the impact acting on the lower leg prevents the lander from rolling downhill.

28

Therefore, a large damping coefficient is preferable for increasing the force applied by the terrain. These two direction changes of the damping coefficient are the reason for the small dependency of $\phi_{\max}$ with ψ. The effect of the twist angle ψ of the lander becomes smaller as the number of legs increases. It thus becomes possible to land on the almost the same incline even if the value of ψ changes for each type of landing gear, but the advantage of landing gear with the variable damper is unchallenged.

The passive-damping landing gear exhibits the smallest incline limit $\phi_{\max}$. The reason for the $\phi_{\max}$ of the passive damper being smaller than $\phi_{\max}$ of the honeycomb is the restoring force of the spring that is installed with a damper in parallel to support the load being acted on by gravity. This spring absorbs kinetic energy when it is compressed, but releases energy when it extends. A honeycomb crush absorbs kinetic energy by deforming; therefore, it does not release energy. However, the lower leg should re-extend after being compressed to prevent any rotating motion. This would be impossible with a honeycomb. The variable damper can satisfy these two conflicting requirements by instantly adjusting its damping force according to the current attitude of the lander.

Figure 17 shows the best and worst cases for the maximum incline $\phi_{\max}$ for which a touchdown is possible. The mean value $\mathrm{mean}_\psi(\phi_{\max})$ increases considerably as the number of legs increases from three to four and it converges to a constant value in the case of the passive damper. For a honeycomb, $\mathrm{mean}_\psi(\phi_{\max})$ increases with five legs and converges with vibration. When the damper is variable, the mean value $\mathrm{mean}_\psi(\phi_{\max})$ increases slightly with seven legs and converges to a constant value. In addition, the minimum case of $\min_\psi(\phi_{\max})$ never become smaller than the maximum case of the passive and honeycomb. This result indicates that we can choose a small number of landing gears with the variable damper, because a shock absorber incorporating the variable damper can prevent tripping when there is only a small number of landing legs.
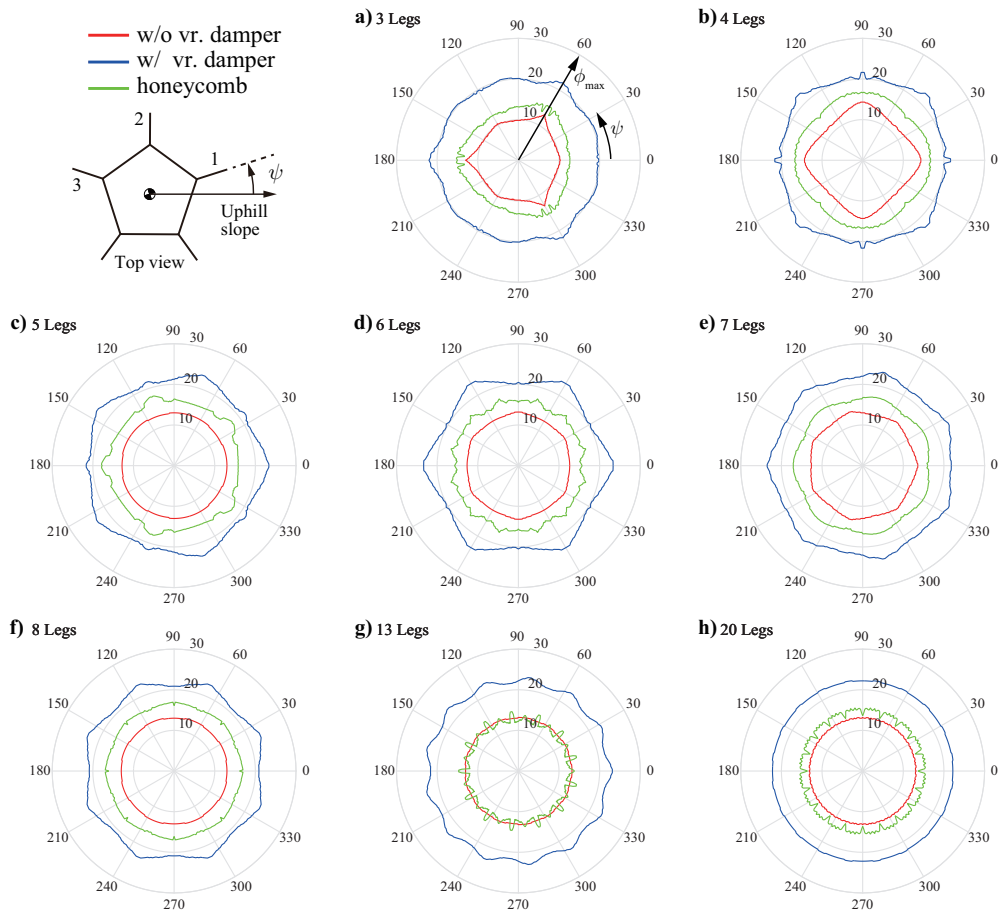
Fig. 16 Maximum incline ϕ_{max} on which touchdown is possible with an N-legged lander. ($N = 3, 4, 5, 6, 7, 8, 13, 20$)
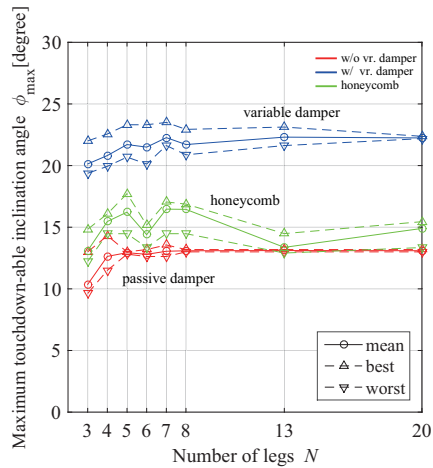

Fig. 17 Maximum and minimum range of incline ϕ_{max} on which a touchdown is possible depends on the twist angle ψ with N legs.

C. Touchdown with lateral velocity

Figure 18 shows the relationship between the maximum lateral velocity $v_{x\max}$ and the twist angle ψ with respect to the direction of the lander velocity. The direction of the radius corresponds to the maximum lateral velocity $v_{x\max}$ while the circumferential direction refers to the mean twist angle ψ. The twist angle ψ is defined as the angle between landing leg no. 1 and the direction of the lateral velocity of the lander. The red line indicates the result obtained with the landing gear without a variable damper (passive), the green line is the result obtained with a honeycomb crush core, and the blue line is the result obtained with the proposed variable damper. Here, the simulation results for three- to twenty-legged lander models are also shown.

The results of our simulations indicate the efficacy of the variable damping landing gear with the proposed control method. The range of lateral velocities for which the lander can still touch down, when using a variable damping landing gear, is superior to the both the passive and honeycomb dampers, regardless of the number of landing legs. When there are three landing legs (Figure 16 a), regardless of the type of the landing legs, the maximum lateral velocity $v_{x\max}$ largely depends on the twist angle ψ. This dependency is shown for every number of landing legs, for both the passive and honeycomb cases. In the case of variable damper, ψ dependency of $v_{x\max}$ becomes unclear. This is also thought to be a result of the switching range of the damping coefficient being the same as in the case of a touchdown on an incline. The difference in the maximum lateral velocity between the passive and the honeycomb dampers is small regardless of the number of landing legs.

The maximum lateral velocities converge to 1.4 m/s when the shock absorber is of either the passive or honeycomb type, as shown in Figure 19. In contrast, the maximum lateral velocity increases to more than 2.0 m/s with the application of the variable damper.

These results of the touchdown simulations confirm the advantages of the variable damper when a touchdown is attempted with a lateral velocity.
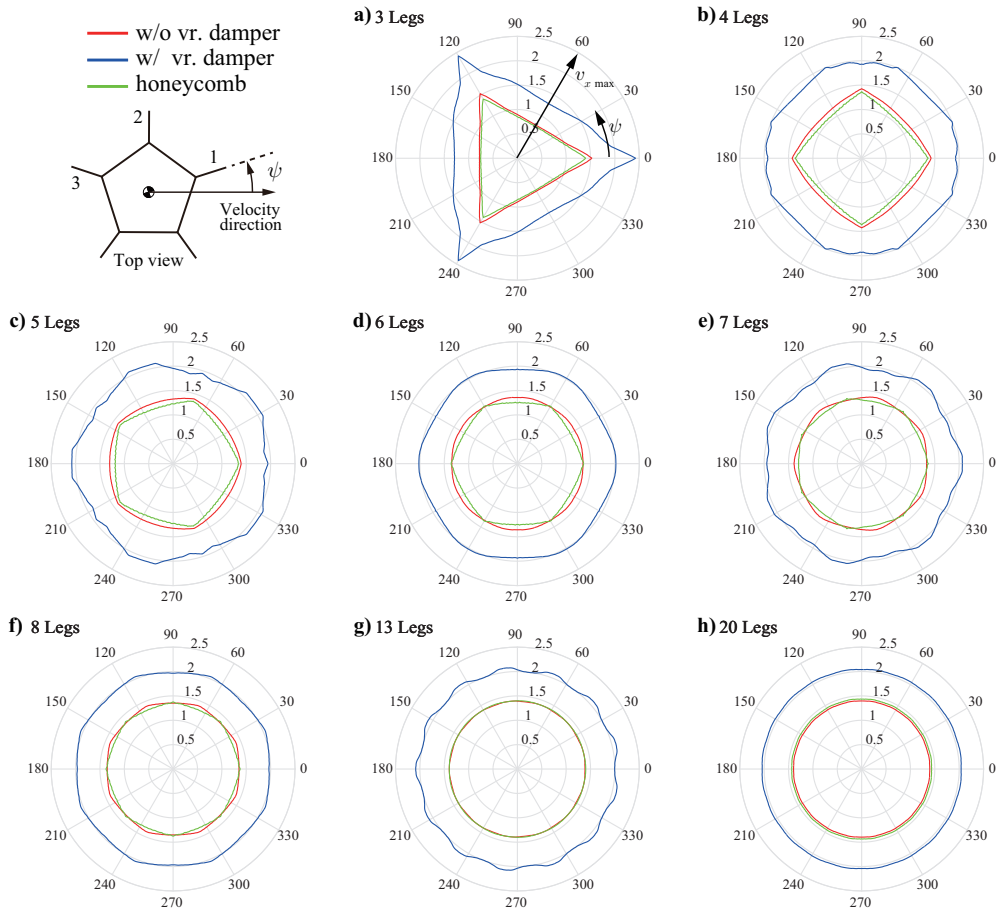
Fig. 18 Maximum lateral velocity $v_{x\mathrm{max}}$ at which touchdown is possible with an N legged lander. $(N = 3, 4, 5, 6, 7, 8, 13, 20)$
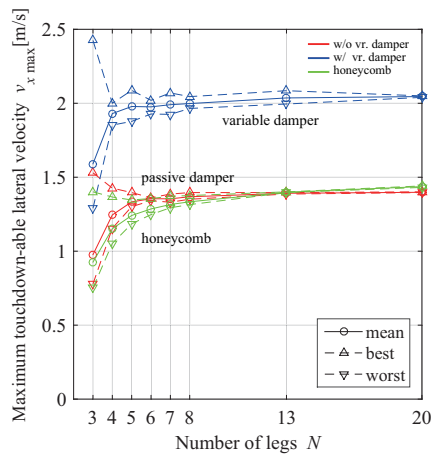

Fig. 19 Maximum and minimum range of lateral velocity $v_{x\mathrm{max}}$ for which touchdown is possible, depending on the twist angle ψ with N legs.

VI.   Conclusion

This paper has proposed a control method for a lunar-planetary lander that relies on a variable-damping shock absorber. First, the control method for the variable-damping shock absorber was derived by application of the Lyapunov function and a three-dimensional dynamics model; it was aimed at reducing the roll angle attitude error. Second, touchdown simulations both with and without a variable damper on the landing gear were carried out. The result obtained for the attitude, force acting on the landing leg, and the control input to the variable damper indicates the effectiveness of the proposed control method for preventing overturning. Furthermore, we investigated the maximum inclination of a planetary surface and which touchdown was possible with the passive, honeycomb, and variable shock attenuation mechanisms. These results indicate that making the damping coefficient large or small across two stages in the real-time feedback control, causes the limit on the incline to become twice that which is possible when using a passive damper. By means of simulation with a range of conditions and configurations, the efficacy of the variable damping landing gear for application to a lunar and planetary landing vehicle capable of negotiating rough terrain was confirmed. In future studies, we intend to test, by means of experiment, a scale model of a lander on an incline, on rocky terrain, on regolith stimulant and another dangerous surface shapes, thus validating the system's ability to prevent the lander from overturning.

Appendix

A1. Nominal damping coefficient and spring constant determination method

It is necessary to determine the nominal damping coefficient c_{nom} and spring constant k_{nom} for a passive landing leg to enable a comparison with the proposed method that uses variable damping. Here, we select the damping ratio $\zeta = 1$ (critical damping) to prevent the vibration of the body. First, we determine the nominal shrinkage of the landing leg d_{nom} by using the contact velocity $v = 3.0\text{m/s}$ and the mass of the lander body $m = 130\text{kg}$. Second, we assume that one spring and damper receives all of the force and thus calculate the total damping coefficient C_{nom} and the total spring constant K_{nom}, these being the values for which all of the lander legs can be thought of as one spring and one damper, shown in Figure 20. The values of C_{nom} and K_{nom} are determined such that $d_{max} = d_{nom}$. Finally, the total damping coefficient and the total spring constant are

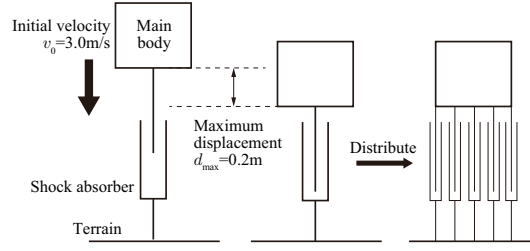**Fig. 20 Nominal displacement definition of shock absorber.**

distributed to the each landing leg. Therefore, each leg has c_{nom} and k_{nom} as given by

$$c_{\text{nom}} = C_{\text{nom}}/N, \ k_{\text{nom}} = K_{\text{nom}}/N.$$

A2. Crush force determination method

A honeycomb crush core shock attenuation mechanism is defined as follows. First, we consider the case where one crush core absorbs all of the kinetic energy. The nominal shrinkage of the crush core d_{nom} is determined in the same way as the nominal displacement of the spring-damper. Second, the product of the crush force and the shrinkage $F_Y \cdot d_{\text{nom}}$ equals the absorbed energy that is equal to the initial kinetic energy before touch-down $(E = 1/2 m \boldsymbol{v}^\top \boldsymbol{v}, \ |\boldsymbol{v}| = 3.0 \text{ m/s})$, thus the crush force is determined as

$$F_Y = E/d_{\text{nom}}.$$

Third, to express the stiffness of the honeycomb, the elastic force acting on the honeycomb when the displacement is smaller than 0.2% $(d < d_Y)$ of initial length. In this case, the elastic force F is proposed for to the displacement d. The stiffness coefficient K_f is given as

$$K_f = F_Y/d_Y.$$

Finally, the crush force is distributed to each landing leg. Therefore, each leg is subject to a crush force f_Y and K_f, as shown in,

$$f_Y = F_Y/N, \ k_f = K_f/N.$$

If the displacement velocity is larger than zero or the displacement is larger than zero, the crush force does not act.

[1] Sawai, S., Mizuno, T., Fukuda, S., Nakaya, K., Haruyama, J., Okada, T., Nakatsuka, J., Saiki, T., Yasumitsu, R., and Morishima, K., "Conceptual Study on SLIM: Smart Lunar Landing Technology Demonstrator," *Proceedings of 28th International Symposium on Space Technology and Science*, 2011, Paper No.2011-f-21.

[2] Hashimoto, T., Hoshino, T., Tanaka, S., Otsuki, M., Otake, H., and Morimoto, H., "Japanese moon lander SELENE-2-Present status in 2009," *Acta Astronautica*, Vol. 68, No. 78, 2011, pp. 1386 – 1391. doi: 10.1016/j.actaastro.2010.08.027

[3] Haruyama, J., Sawai, S., Mizuno, T., Yoshimitsu, T., Fukuda, S., and Nakatani, I., "Exploration of Lunar Holes, Possible Skylights of Underlying Lava Tubes, by Smart Lander for Investigating Moon (SLIM)," *Transactions of The Japan Society for Aeronautical and Space Sciences, Aerospace Technology Japan*, Vol. 10, No. ISTS28, 2012, pp. Pk_7–Pk_10. doi: 10.2322/tastj.10.Pk_7

[4] Taguchi, K., Hashimoto, T., and Otsuki, M., "Dynamic Touchdown Control for Safe and Precise Landing Using Active Landing Leg," *Proceedings of 53th Space Sciences and Technology Conference*, 2009, Paper No. 2D05.

[5] Maeda, T., Hashimoto, T., Otsuki, M., and Sakai, S., "Development of Active Controlled Landing Gear Experiment System for theLunar–Planetary Lander," *Proceedings of 11th Conference on Motion and Vibration Control*, 2012, Paper No. B112.

[6] Shigeto, S., Fujimoto, H., Hori, Y., Otsuki, M., and Hashimoto, T., "Fundamental Research on Reduction of Impact Forces Using Actively Controlled Landing Gear in Lunar/Planetary Landers," *IEEJ Transactions on Industry Applications*, Vol. 133, No. 3, 2013, pp. 335–341. doi: 10.1541/ieejias.133.335

[7] Hara, S., Watanabe, T., Kushida, Y., Otsuki, M., Yamada, Y., Matsuhisa, H., Yamada, K., Hashimoto, T., and Kubota, T., "Study on Landing Response Control of Planetary Exploration Spacecraft Based on Momentum Exchange Principles," *Transactions of the Japan Society of Mechanical Engineers, Series C (in Japanese)*, Vol. 78, No. 792, 2012, pp. 2781–2796. doi: 10.1299/kikaic.78.2781

[8] Kushida, Y., Hara, S., Otsuki, M., Yamada, Y., Hashimoto, T., and Kubota, T., "Robust Landing Gear System Based on a Hybrid Momentum Exchange Impact Damper," *Journal of Guidance, Control, and Dynamics*, Vol. 36, No. 3, 2013, pp. 776–789. doi: 10.2514/1.58373

[9] Saeki, N., Hara, S., Otsuki, M., Watanabe, T., and Yamada, Y., "Base-Extension Separation Mechanism for Planetary Exploration Spacecraft Landing," *Transactions of The Japan Society for Aeronautical and Space Sciences, Aerospace Technology Japan*, Vol. 12, No. ISTS29, 2014, pp. Pd_91–Pd_100. doi: 10.2322/tastj.12.Pd_91

[10] Manivannan, V., Langley, J. P., Costello, M. F., and Ruzzene, M., "Rotorcraft Slope Landings with Articulated Landing Gear," 2013, Paper No. AIAA 2013–5160. doi: 10.2514/6.2013-5160

[11] Kiefer, J., Ward, M., and Costello, M., "Rotorcraft Hard Landing Mitigation Using Robotic Landing Gear," *Journal of Dynamic Systems, Measurement, and Control*, Vol. 138, No. 3, 2016, pp. 031003. doi: 10.1115/1.4032286

[12] Rippere, T. B. and Wiens, G. J., "An approach to designing passive self-leveling landing gear with application to the Lunar Lander," *Proceedings of the 40th Aerospace Mechanisms Symposium, NASA Kennedy Space Centre*, 2010.

[13] Maeda, T., Otsuki, M., and Hashimoto, T., "Overturning protection control of lunar-planetary lander with semi-active shock absorber," *Transactions of the JSME (in Japanese)*, Vol. 80, No. 816, 2014, pp. DR0235–DR0235. doi: 10.1299/transjsme.2014dr0235

[14] Sakai, S., Sawai, S., Fukuda, S., Nakaya, K., Sato, E., Kunugi, M., and Yasumitsu, R., "Smart lander for Investigating Moon (SLIM): Demonstration of smart Lunar landing technology with small spacecraft," *Proceedings of 57th Space Sciences and Technology Conference*, 2013, Paper No. 3F06.

[15] Dyke, S., Spencer Jr, B., Sain, M., and Carlson, J., "Modeling and control of magnetorheological dampers for seismic response reduction," *Smart materials and structures*, Vol. 5, No. 5, 1996, pp. 565.

[16] Ho, C., Lang, Z., Sapiński, B., and Billings, S., "Vibration isolation using nonlinear damping implemented by a feedback-controlled MR damper," *Smart Materials and Structures*, Vol. 22, No. 10, 2013, pp. 105010.

[17] "LORD Technical Data RD-8040-1 and RD-8041-1 Dampers," Accessed on November 2015, www.lordfulfillment.com/upload/DS7016.pdf.

[18] Christensen, E. M., Batterson, S. A., Benson, H. E., Choate, R., Hutton, R. E., Jaffe, L. D., Jones, R. H., Ko, H. Y., Schmidt, F. N., Scott, R. F., Spencer, R. L., and Sutton, G. H., "Lunar surface mechanical properties," *Journal of Geophysical Research*, Vol. 73, No. 22, 1968, pp. 7169–7192. doi: 10.1029/JB073i022p07169

[19] Schiehlen, W., "Multibody system dynamics: roots and perspectives," *Multibody system dynamics*, Vol. 1, No. 2, 1997, pp. 149–188. doi: 10.1023/A:1009745432698

[20] Herr, R. W. and Leonard, H. W., "Dynamic model investigation of touchdown stability of lunar-landing vehicles," *NASA Technical note TN D-4215*, 1967.

[21] Herr, R. W., Leonard, H. W., and Walton, W. C., "Studies of touchdown stability for lunar landing vehicles," *Journal of Spacecraft and Rockets*, Vol. 1, No. 5, 1964, pp. 552–556. doi: 10.2514/3.27696